

High-visibility ghost imaging with phase-controlled discrete classical light sources

Xueying Wu(仵雪滢), Yue Zhao(赵岳), and Liming Li(李利明)

Citation: Chin. Phys. B, 2024, 33 (**7**): 074202. DOI: 10.1088/1674-1056/ad4631
Journal homepage: http://cpb.iphy.ac.cn; http://iopscience.iop.org/cpb

What follows is a list of articles you may be interested in

Defogging computational ghost imaging via eliminating photon number fluctuation and a cycle generative adversarial network

Yuge Li(李玉格) and Deyang Duan(段德洋)
Chin. Phys. B, 2023, 32 (**10**): 104203. DOI: 10.1088/1674-1056/acd8b2

Optical encryption scheme based on spread spectrum ghost imaging

Jin-Fen Liu(刘进芬), Yue Dong(董玥), Le Wang(王乐), and Sheng-Mei Zhao(赵生妹)
Chin. Phys. B, 2023, 32 (**7**): 074202. DOI: 10.1088/1674-1056/acbf27

Principle of subtraction ghost imaging in scattering medium

Qin Fu(付芹), Yanfeng Bai(白艳锋), Wei Tan(谭威), Xianwei Huang(黄贤伟), Suqin Nan(南苏琴), and Xiquan Fu(傅喜泉)
Chin. Phys. B, 2023, 32 (**6**): 064203. DOI: 10.1088/1674-1056/acb202

A probability theory for filtered ghost imaging

Zhong-Yuan Liu(刘忠源), Shao-Ying Meng(孟少英), and Xi-Hao Chen(陈希浩)
Chin. Phys. B, 2023, 32 (**4**): 044204. DOI: 10.1088/1674-1056/ac981e

Ghost imaging based on the control of light source bandwidth

Zhao-Qi Liu(刘兆骐), Yan-Feng Bai(白艳锋), Xuan-Peng-Fan Zou(邹璇彭凡), Li-Yu Zhou(周立宇), Qin Fu(付芹), and Xi-Quan Fu(傅喜泉)
Chin. Phys. B, 2023, 32 (**3**): 034210. DOI: 10.1088/1674-1056/ac6edd

---

High-visibility ghost imaging with phase-controlled discrete classical light sources

Xueying Wu(仵雪滢), Yue Zhao(赵岳), and Liming Li(李利明)†

School of Physics and Optoelectronic Engineering, Shandong University of Technology, Zibo 255049, *China*

(Received 12 March 2024; revised manuscript received 27 April 2024; accepted manuscript online 2 May 2024)

We take phase modulation to create discrete phase-controlled sources and realize the super-bunching effect by a phase-correlated method. From theoretical and numerical simulations, we find the space translation invariance of the bunching effect is a key point for the ghost imaging realization. Experimentally, we create the orderly phase-correlated discrete sources which can realize high-visibility second-order ghost imaging than the result with chaotic sources. Moreover, some factors affecting the visibility of ghost image are discussed in detail.

Keywords: ghost imaging, high visibility, space translation invariance

PACS: 42.30.–d, 42.79.Hp, 07.60.Ly **DOI:** 10.1088/1674-1056/ad4631

1. Introduction

As a promising imaging technology, ghost imaging (GI) has developed for more than two decades.[1,2] Noted worthily, retrieving GI needs light-intensity correlation measurement between two channels, a distinct difference compared with traditional first-order intensity imaging. In the GI scheme, one channel collects the total light transmitted (or reflected[3,4]) by the object with a bucket detector and the other channel records the dynamic structural lighting field on the mirror plane of the object. Actually, if the wavefront of the source in the classical light GI scheme is completely known, the dynamic structural lighting field on the object plane is a priori based on the Huygens–Fresnel diffraction integral theory[5] so that the GI scheme changes from the two channels correlation imaging to the single-pixel imaging (SPI).[6–8]

The first GI experiment[9] was carried out by the quantum two-photon entangled photon pairs in 1995. Due to the extremely weak intensity and costly detection system of entangled sources, some practical applications are difficult to implement such as quantum lithography or standoff imaging. Later, people found the classical source can completely replace the quantum entangled source to realize the GI,[10–15] except the visibility, a key criterion of imaging quality. Compared with 100% achieving theoretically with the quantum entangled source,[9,11,12] the maximum value of visibility for second-order thermal light ghost imaging (TLGI) is 33.3% in theory only for a point-like object. With a complex object used in practical application, the visibility will be extremely low so the application of TLGI is limited. The fundamental reason for the low-visibility of TLGI is due to the background-peak ratio 1/2 in the second-order bunching effect,[16,17] which is the point spread function (PSF) of GI system actually.[15,18–20] To achieve high-visibility TLGI, researchers have sought modifying imaging algorithms[20–25] or fabricating the lighting sources.[26–30] Moreover, the n-order ($n \geq 3$) TLGI[31–40] is also effective for the visibility because of the background-peak ratio theoretically suppressed to $1/(n!)$ in n-order bunching effect with thermal light.[41] In fact, some higher-order correlation algorithms can also help improve the visibility[40,42] and resolution[43] of ghost interference.

Just as the authors in Ref. [44] pointed out, these digital devices (light modulator or light detector) in computational ghost imaging (CGI) affect the statistical behaviors of intensity of light on the detection plane so that the visibility of ghost imaging is variable. Actually, the phase modulation in our paper inevitably affects the statistical behaviors of light on the detection plane. However, We would like to emphasize that the super-bunching of the second-order coherence of light and the high-visibility of ghost image in our paper are originating from the interference of multiple inphase indistinguishable two-photon paths by the phase modulation on the sources, which is a new degree of freedom to modulate high-order coherence of light field and is also a new physical perspective comparing with the statistical behaviors of light on the detection plane as discussed in Ref. [44].

From the second-order interference perspective, the visibility of spatial TLGI can be improved if suppressing the background-peak ratio of the spatial bunching effect, such as the super-bunching effect.[45–50] Actually, there is also a premise that the super-bunching effect can improve the visibility of ghost images, which has never been raised in a paper as far as we know. The super-bunching effect should satisfy the space translation invariance, i.e., the correlation intensity of the second-order fringes determined by the relative position between two detectors rather than the specific position of detectors.

†Corresponding author. E-mail: liliming@sdut.edu.cn

© 2024 Chinese Physical Society and IOP Publishing Ltd

In this paper, we constructed phase-controlled discrete classical sources which achieve a one-channel high-visibility second-order GI. Theoretically, we analyzed the super-bunching effect and whether or not it satisfies the space translation invariance from those phase-controlled sources. Then, the GI capabilities of those phase-controlled sources are compared in detail by numerical simulation. Experimentally, we demonstrated the visibility of GI results with two-dimensional (2D) orderly phase-correlated sources higher than those with the chaotic case. In the end, we discussed some factors affecting the visibility of GI, such as the size of the imaging object, the order n in the n-order GI, and the point number in phase-controlled discrete sources, respectively.

2. Theory

The interference and diffraction of classical light can be analyzed from the perspective of photon interference, so the high-order interference with classical light is no exception. Figure 1 shows a schematic diagram to study the first- and second-order far-field coherence of N equidistant discrete point sources (S_1, S_2, …, S_N), in which f is the focal length of the lens and D_v ($v = 1, 2$) is a single-photon detector in the far-field observation plane (or the Fraunhofer zone of sources). Then, the second-order spatial correlation can be performed with the coincidence counting (CC) system. For any two point sources in the discrete sources such as S_i and S_j, when the initial phase is completely random and independent, it is evident that two point sources are first-order incoherent over long periods,[5] but one can observe second-order interference fringes.[51–53]

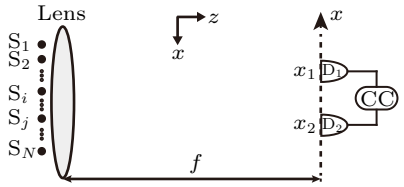


Fig. 1. Fundamental scheme to study the first- and second-order coherence with N point sources (S_1, S_2, …, S_N). f: the focal length of the lens. D_v ($v = 1, 2$): photon-detector. CC: coincidence counting system.

From the two-photon paths perspective,[54–57] those valid coincidence counts will consist of two parts: (i) detected photon pairs originating from a single point source ($S_iD_1S_iD_2$ or $S_jD_1S_jD_2$) which is the self-correlation part of the second-order correlation function only resulting in a constant background; (ii) detected photon pairs originating from different point sources ($S_iD_1S_jD_2$ or $S_iD_2S_jD_1$) which is the cross-correlation part of the second-order correlation function fostering the interference fringes. Here, $S_iD_{v_1}S_jD_{v_2}$ stands for the two-photon paths: photon S_i goes to detector D_{v_1} while photon S_j goes to detector D_{v_2}, where $i, j \in \{1, 2, \ldots, N\}$ and $v_1, v_2 \in \{1, 2\}$. In fact, $S_iD_1S_jD_2$ and $S_iD_2S_jD_1$ are indistinguishable twins two-photon paths, which is the key point of the high-order interference. Fundamentally, the second-order interference is the result of the superposition of multiple two-photon paths, whose phase factor dominates the interference performance. The phase factor includes two parts: one is the source part which is decided by the initial phase of photon pairs and the other is the propagation part which depends on the two-photon paths from sources to detectors. In general, the source part decides whether the interferometer works or not and the propagation part decides constructive or destructive superposition of multiple two-photon paths. For example, the characteristics of the second-order bunching effect depend on the light source itself but the position of bunching peak relies on the displacement between two point detectors.

The extension from two independent point sources to N equidistant independent point sources is straightforward.[18] At this moment, the instantaneous electric field amplitude on the detection plane in the paraxial approximation can be expressed as

$$E(x) = C\sum_{l=1}^{N} \exp\left[-\mathrm{i}\,(l-1)\,\frac{kxd}{f}\right] \mathrm{e}^{-\mathrm{i}\varphi_l}, \tag{1}$$

where C is an insignificant scale factor, $k = 2\pi/\lambda$ is the wave vector of the wavelength λ, d is the displacement between adjacent points of the discrete sources, f is the focal length of the lens, and φ_l ($l = 1, 2, \ldots, N$) is the initial phase of the l-th point source, which is completely random and uniformly distributed within $[0, 2\pi)$, respectively. Thus, the self-correlation first-order and normalized second-order spatial correlation functions in the far-field detection plane can be expressed as[18]

$$G^{(1)}(x) = \langle E^*(x)E(x)\rangle = C^2N, \tag{2}$$

$$\begin{aligned} g^{(2)}(x_1,x_2) &= \frac{\langle E^*(x_1)E(x_1)E^*(x_2)E(x_2)\rangle}{\langle E^*(x_1)E(x_1)\rangle\langle E^*(x_2)E(x_2)\rangle} \\ &= 1+\frac{1}{N^2}\frac{\sin^2(N\pi d(x_1-x_2)/(\lambda f))}{\sin^2(\pi d(x_1-x_2)/(\lambda f))}, \end{aligned} \tag{3}$$

where $\langle\cdots\rangle$ stands for the ensemble average. Here, the periodic bunching peak[18] originates from the discrete character of source. Because of the first-order incoherence among those N point sources, the phase factor of every two-photon paths is totally random except for the twins two-photon paths originating from a pair of point sources. Hence, the maximum number of inphase indistinguishable two-photon paths is 2, which is irrelevant to the total point number N of the source. The visibility $V = (g^{(2)}_{\max} - g^{(2)}_{\min})/(g^{(2)}_{\max} + g^{(2)}_{\min})$ of second-order interference fringes expressed by Eq. (3) is 33.3%, where $g^{(2)}_{\max}$ and $g^{(2)}_{\min}$ are maximum and minimum value of $g^{(2)}(x_1, x_2)$, respectively. Actually, equation (3) also gives the second-order ghost image for a point-like object.

However, the number of indistinguishable two-photon paths will increase if the initial phase of the discrete point

source has some correlation, such as the phase $\varphi_l = l\theta$ satisfying the orderly arithmetic progression,[57] where θ is randomly and uniformly distributed within [0, 2π). Now, those two-photon paths coming from those pairs of point sources (i, j) with equal $(i+j)$ are inphase and indistinguishable in theory. At this moment, the maximum number of inphase indistinguishable two-photon paths is $2N$ for the case $i+j = N+1$. The instantaneous electric field amplitude on the detection plane in the paraxial approximation can be expressed as

$$E(x) = C' \sum_{l=1}^{N} \exp\left[-\mathrm{i}\left(\chi(l)-1\right)\frac{kxd}{f}\right] \mathrm{e}^{-\mathrm{i}l\theta}, \tag{4}$$

where C' is an insignificant scale factor and $\chi(l)$ is the location number of the source initial phase $l\theta$. For the orderly arithmetic progression phase $\varphi_l = l\theta$, $\chi(l)$ is equal to l. Obviously, the first-order self-correlation spatial correlation function in the far-field detection plane derives from incoherent superposition and can be expressed as

$$G^{(1)}(x) = \langle E^*(x) E(x) \rangle = C'^2 N. \tag{5}$$

After precluding the self-correlation first-order interference, one can observe the second-order interference fringes[57]

$$g^{(2)}(x_1, x_2) = \sum_{s=1-N}^{N} \frac{\sin^2(s\pi d(x_1 - x_2)/(\lambda f))}{N^2 \sin^2(\pi d(x_1 - x_2)/(\lambda f))}. \tag{6}$$

Here, the maximum of $g^{(2)}(x_1, x_2)$ is $\frac{1}{N^2}\sum_{s=1-N}^{N} s^2 = \frac{2N^2+1}{3N}$ at the case $x_1 - x_2 = \mathcal{N}\lambda f/d$ between two point detectors on the detected plane, where $\mathcal{N}$ is an integer $(0, \pm1, \pm2, \ldots)$. Here, the visibility of the second-order interference fringes is $(N^2-1)/(N^2+2)$, which is decided by the total point number N of source.[57] Interestingly, it can be seen that this orderly phase-correlated discrete sources shows the potential to achieve high-visibility ghost image.

Furthermore, any one of factorial$(N) = N!$ equidistant discrete point sources created by all permutations of arithmetic progression phase $(\theta, 2\theta, \ldots, N\theta)$ can construct the multi-path second-order interference. Due to the disorderly permutation of the sources' phase, the diffraction light field will exhibit rich second-order interference patterns. According to Eq. (5), the self-correlation first-order interference will be erased for the equidistant discrete point sources with arbitrary phase permutation. After precluding the first-order interference, because of the complementary between the first-order and the second-order interference patterns,[58,59] the normalized second-order correlation function here can be expressed as

$$\begin{aligned} & g^{(2)}(x_1, x_2) \\ &= \left\langle \left| \sum_{l=1}^{N}\sum_{m=1}^{N} \exp\left[\mathrm{i}\left(\chi(l)-1\right)\frac{kdx_1}{f}\right] \right.\right. \\ &\quad \left.\left. \times \exp\left[\mathrm{i}\left(\chi(m)-1\right)\frac{kdx_2}{f}\right] \mathrm{e}^{\mathrm{i}(l+m)\phi} \right|^2 \right\rangle \\ &= \sum_{s=2}^{N+1} \left| \sum_{l=1}^{s-1} \exp\left[\mathrm{i}\left(\chi(l)-1\right)\frac{kdx_1}{f}\right] \mathrm{e}^{\mathrm{i}(\chi(s-l)-1)\frac{kdx_2}{f}} \right|^2 \\ &\quad + \sum_{s=N+2}^{2N} \left| \sum_{l=s-N}^{N} \exp\left[\mathrm{i}\left(\chi(l)-1\right)\frac{kdx_1}{f}\right] \right. \\ &\quad \left. \times \exp\left[\mathrm{i}\left(\chi(s-l)-1\right)\frac{kdx_2}{f}\right] \right|^2. \end{aligned} \tag{7}$$

One can see that different $\chi(l)$ of phase sequence lead to a different second-order interference pattern. Thus, the normalized second-order correlation function $g^{(2)}(x_1, x_2)$ cannot be expressed as the function of $x_1 - x_2$, except Eq. (6) from the orderly phase-correlated sources. Consequently, the space translation invariance is destroyed as the phase permutation is disorderly, but the super-bunching effect still appears in some detection cases. At this point, if disorderly phase modulation scheme is adopted, the GI capability of the phase-controlled sources will be weakened because the GI scheme cannot create the point-to-spot correlation. Below, we will confirmed this point by the numerical experiment. Although the above theoretical discussion is restricted to one-dimensional (1D) sources, this assumption does not influence the generality of the approach since the results can be directly extended to 2D sources. In the following text, we will compare the second-order interference patterns and GI capability of discrete point sources with a completely random phase, the orderly and disorderly arithmetic progression phase, respectively.

3. Numerical simulation and experiment

Now, let us consider the second-order interference and GI schemes with phase-controlled sources. Figure 2(a) shows the setup of the second-order interference with a phase-controlled source. A single-mode continuous-wave laser beam with a wavelength $\lambda = 780$ nm was expanded, collimated, and reshaped through a beam expander (BE) and a square slot (SS). The reshaped beam was reflected by a 50:50 non-polarized beam splitter (BS) and then immediately incident normally on a phase-only spatial light modulator (SLM, PLUTO 1080P from HOLOEYE Photonics AG, Germany, an element pixel size of 8 μm×8 μm). The phase-encoded beam successively transmits through the BS and a lens L1 and is collected by a charge-coupled device (CCD, Beamage-CCD23 with 1360 × 1024 pixels, an element pixel size of 6.45 μm×6.45 μm) camera. Here the focal length of L1 is f_1 = 80 cm and the CCD was put on the rear focal plane of L1. One notes that the reshaped laser beam together with the SLM acts as the phase-controlled source. Notably, due to the discrete character of the phase-controlled source, one arm GI scheme without the diffraction integral operation can be built when a $2f_2$–$2f_2$ imaging setup

replaces the CCD in the second-order interference scheme as shown by the figure 2(b), where f_2 is the focal length of lens L2. A detailed description about GI realization can be found in those references.[18,20]

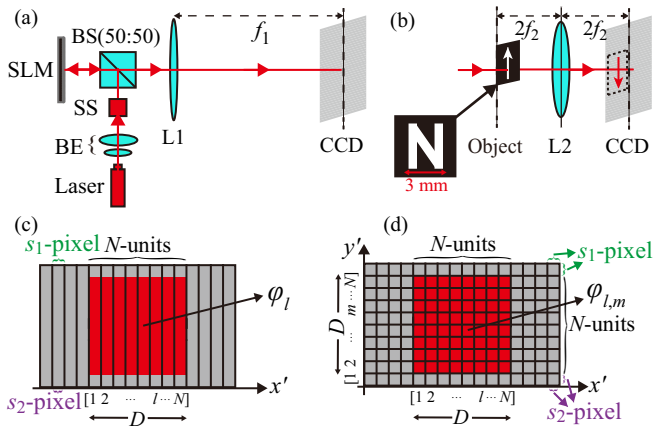


Fig. 2. (a) Schematic diagram of the experimental setup for the interference scheme. BE: beam expander; SS: square slot; BS: beam splitter; SLM: spatial light modulator; CCD: charge-coupled device. f_1 is the focal length of the lens L1. (b) A $2f_2$–$2f_2$ imaging system. f_2 is the focal length of the lens L2. (c) and (d) The panels of pure-phase SLM showing the phase configuration of the designed 1D and 2D phase-controlled discrete light sources, respectively. The red areas on the panels indicate the light field on the SLM plane.

Figures 2(c) and 2(d) show the spatial distribution of the initial phase of the 1D and 2D phase-controlled sources, respectively. In the 1D case, we combined the neighboring s_1 pixels of SLM along the x' dimension as a unit whose middle s_2 pixels (as the effective part) loaded with the same phase while the rest part (s_1–s_2 pixels) of the unit is opaque in the numerical simulation so that the CCD only collects those beams reflected by those effective parts. The middle s_2 pixels in the unit act as a single slit source. What is more, in the 2D case we combined the neighboring $s_1 \times s_1$ pixels of SLM as a unit whose middle $s_2 \times s_2$ pixels (as the effective part) were loaded with the same phase, and the rest parts are loaded with the blazed grating-phase in the experimental demonstration. In this way, only the light beams reflected from the effective part were collected by the CCD on the detection plane. The middle $s_2 \times s_2$ pixels in the unit act as a single square point source. In the setup, the width D of the SS was adjustable which determines the size of the light wavefront in the SLM panels (see the red areas in Figs. 2(c) and 2(d)).

Figure 3 shows the 2D distribution of the numerical simulation result of the normalized second-order interference $g^{(2)}(x_1,x_2)$ with four kinds of phase-controlled sources: independent chaotic sources (a), orderly phase-correlated sources (b), the first (c) and the second (d) kinds of disorderly phase-correlated sources, respectively. Those four kinds of 1D phase-controlled sources in the numerical simulation are built by $N = 10$ equidistant slit sources and have the same physical unit $s_1 = 20$ and $s_2 = 2$. For the independent chaotic sources, the initial phase φ_l ($l = 1,2,\ldots,N$) of l-th point source is completely random and uniformly distributed within $[0,2\pi)$. However, the initial phase φ_l in the orderly phase-correlated sources is $l\theta$, where θ is completely random and uniformly distributed within $[0,2\pi)$. One note that the number of all permutations of the initial phase $[\varphi_1,\varphi_2,\ldots,\varphi_N]$ is $N! = 3628800$. Here we randomly select two arrangement schemes to construct these two disorderly phase-correlated sources. For the first and the second kinds of disorderly phase-correlated sources, the permutation $\chi_1(l)$ and $\chi_2(l)$ are $[1,2,9,7,5,3,4,10,8,6]$ and $[1,10,3,4,6,5,9,8,7,2]$, respectively.

In the numerical simulation, total 10000 frames of self-correlation first-order intensity were calculated by the Huygens–Fresnel diffraction integrals and then the normalized second-order interference can be calculated. Compared with the independent chaotic sources, those phase-correlated sources whether orderly arranged or not can create multiple in-phase indistinguishable two-photon paths leading to the super-bunching effect $g^{(2)}(0,0) > 2$. What is more, as shown by Figs. 3(a) and 3(b), those normalized second-order correlation function originating from the independent chaotic sources and the orderly phase correlated sources satisfies the space translation invariance, namely, the intensity of the bunching effect determined by the relative position between two detectors rather than the specific position of two detectors. Graphically, the intensity of the second-order fringes is invariant in the cross-section at the $x_1 - x_2 = C''$ direction, where C'' is an arbitrary constant. However, the second-order interference originated from those two kinds of disorderly phase-correlated sources does not satisfies the space translation invariance as shown by Figs. 3(c) and 3(d).

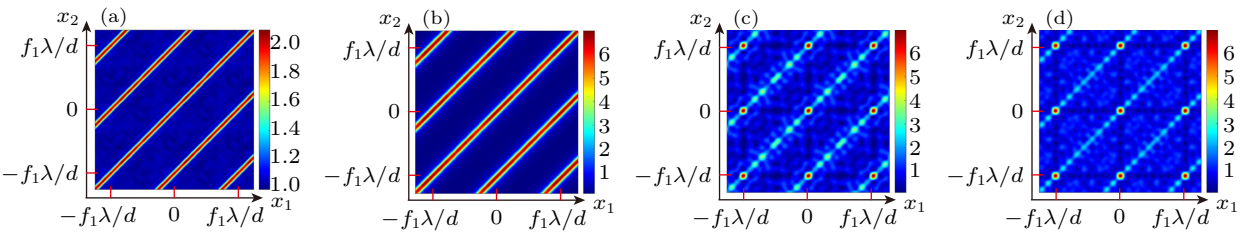


Fig. 3. The 2D distribution of the numerical simulation of the normalized second-order correlation function with four kinds of 1D phase-controlled sources: independent chaotic point sources (a), orderly phase-correlated sources (b), the first (c) and the second (d) kinds of disorderly phase-correlated sources, respectively.

Interestingly, one sees that the second-order interference fringes with those four kinds of phase-controlled sources is periodic either along the x_1 or x_2 coordinate axis due to the particular discrete characteristic of sources.[18] Because of the same distance d between the nearest neighboring discrete slit points in those four kinds of phase-controlled sources, the period of the normalized second-order correlation function shown in Fig. 3 is the same and equal to $\lambda f_1/d$.

To demonstrate the necessity of the space translation invariance of the bunching effect for the GI formation, figure 4 shows the numerical simulation of the second-order GI profiles, created by the one-arm computing GI with those four kinds of phase-controlled sources. Detailed operations can be seen in those Refs. [18,20]. Here, the n-order ghost image $\mathrm{GI}^{(n)}(x)$ on the image plane of the $2f_2$–$2f_2$ imaging system can be calculated through[33,36]

$$\mathrm{GI}^{(n)}(x)=\frac{\dfrac{1}{10000}\displaystyle\sum_{i=1}^{10000}\left(I_i(x)\times BI_i^{n-1}\right)}{\langle I(x)\rangle\langle BI\rangle^{n-1}}, \tag{8}$$

where 10000 is the number of total frames of the intensity distribution, $I_i(x)$ is the first-order intensity of the i-th frame, BI_i is the bucket intensity signal originated by the sum of the transmitted light in object image area on CCD detected plane, $\langle I(x)\rangle$ and $\langle BI\rangle$ are the ensemble average over all measured $I_i(x)$ and BI_i, respectively. In Fig. 4, the black solid line and the blue dotted line are the GI profiles with the independent chaotic sources and the orderly phase-correlated sources, respectively. The gray blocks at the bottom in Fig. 4 represent the 0–1 amplitude object with clear equal interval slits. The value of the black solid line of GI profiles is distributes in $[1, 1.33]$ with the independent chaotic sources. However, due to the super-bunching effect ($g^{(2)}(x_1=x_2)=7.0$) with the orderly phase-correlated sources, it is possible that the value of GI is larger than 2 with a relatively simple imaging object. Here, the maximum value of the blue dotted line of ghost image is 2.22 in Fig. 4. One sees that those two kinds of phase-controlled light sources can realize GI, and the GI originated from the orderly phase-correlated sources show a high-visibility than the chaotic case. In addition, due to the discrete characteristic of those phase-correlated sources, those GI profiles can achieve ghost image copy in the transverse dimension.

What is more, the red hollow triangles and the green hollow squares in Fig. 4 are the GI profiles with the first and the second disorderly phase-correlated sources, respectively. Obviously, those two kinds of disorderly phase-correlated sources are not suitable for the source in the GI scheme because the imaging scheme cannot create the point-to-spot correlation between the object plane and the image plane. Thus, the space translation invariance of bunching effect is crucial and indispensable for the GI established.

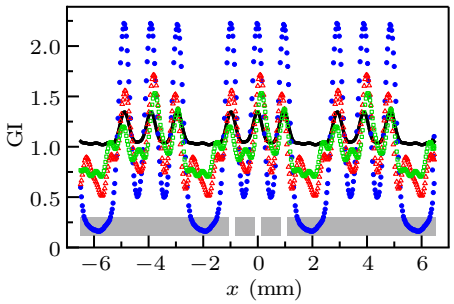


Fig. 4. The numerical simulation of the second-order ghost image profiles with four kinds of phase-controlled sources: the independent chaotic sources (the black solid line), the orderly phase-correlated sources (the blue dotted line), the first (the red hollow triangles), and the second (the green hollow squares) disorderly phase-correlated sources, respectively. The gray blocks at the bottom represent the 0–1 amplitude object with clear equal interval slits.

Considering that the disorderly phase-correlated sources cannot serve as the sources in GI scheme, we only give the experimental demonstration the high-visibility of the second-order GI with 2D orderly phase-correlated sources than the chaotic case. Here, we adopted 2D phase modulation with $s_1=20$ and $s_2=10$ as shown by Fig. 2(d). Furthermore, the phase $\varphi_{l,m}$ loaded on the (l,m)-th discrete point source was randomly and uniformly distributed within [0, 2π) for the phase-independent discrete chaotic source. For the orderly phase-correlated sources, the phase $\varphi_{l,m}$ was $(mN+l)\theta$, where the phase θ is randomly and uniformly distributed within [0, 2π) and N is point number in a single dimension. Here, the width D of the light spot in the SLM panel was set as 3.35 mm leading to an $N\times N$ point sources array, where $N=21$. What is more, a binary 0–1 object "**N**" with a letter size 3 mm and a line width 500 μm was located at the rear focal plane of L1. Detailed experimental operations can be seen in those Refs. [18,20].

Figures 5(a) and 5(b) show the experimental second-order GI results, normalized as $\mathrm{GI}/\mathrm{GI}_{\max}$, with 2D independent chaotic sources and 2D orderly phase-correlated sources, respectively. Here, $\mathrm{GI}_{\max}$ is the maximum of GI result. To demonstrate clearly the high-visibility capability of the 2D orderly phase-correlated sources than the chaotic in ghost imaging scheme, figure 5(c) gives the corresponding horizontal cross-section. The blue solid curve and the red hollow triangles in Fig. 5(c) are the cross-section of distribution of ghost images at $(x, y=0)$ direction in Figs. 5(a) and 5(b), respectively. One notes that the smaller $(\mathrm{GI}/\mathrm{GI}_{\max})_{\min}$ is, the higher visibility of ghost image,[36] where $(\mathrm{GI}/\mathrm{GI}_{\max})_{\min}$ is the minimum of the normalized ghost image $(\mathrm{GI}/\mathrm{GI}_{\max})$. Here, a total of 10000 frames intensity distribution with an exposure time of 1.0 ms were grabbed by each camera per plot. In addition, the bucket signal BI_i was obtained through an intensity integration of traditional imaging over the area within the white dashed rectangle shown in Fig. 5. Comparing with the ghost image result $(\mathrm{GI}/\mathrm{GI}_{\max})_{\min}=0.992$ with independent chaotic sources, the ghost image result $(\mathrm{GI}/\mathrm{GI}_{\max})_{\min}=0.84$ with the orderly phase-correlated sources shows a higher visibility.

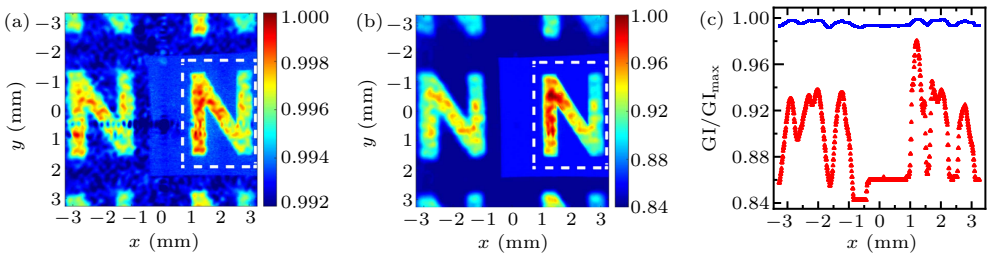


Fig. 5. Experimental results of the normalized second-order ghost image $\mathrm{GI}/\mathrm{GI}_{\max}$ with the 2D independent chaotic sources (a) and the 2D orderly phase-correlated sources (b), respectively. The blue solid curve and the red hollow triangles in panel (c) are the cross-section at $(x, y = 0)$ direction in panels (a) and (b), respectively.

4. Discussion

As we all know, the visibility of images is determined by many factors of imaging scheme. To further show the high-visibility superiority of the GI scheme with orderly phase-correlated sources than the chaotic one, we propose three GI schemes by numerical simulation in the following text. To provide a brief description, we only show the variation of $(\mathrm{GI}/\mathrm{GI}_{\max})_{\min}$ with certain factors.

Figure 6 show three kinds of numerical simulation results of $(\mathrm{GI}/\mathrm{GI}_{\max})_{\min}$ with a rectangular window function object $t(x) = \mathrm{rect}(x/W)$, where W is the window size and $\mathrm{rect}(x)$ is the rectangular function defined as $\mathrm{rect}(x) \equiv \begin{cases} 1, & |x| \le 1/2, \\ 0, & \text{otherwise.} \end{cases}$ Herein, the black hollow triangles and the red hollow squares in Fig. 6 are the simulation data acquired by 10000 exposure frames with the 1D independent chaotic point sources (abbreviated as the Chaotic hereafter) and the orderly phase-correlated sources (abbreviated as the Orderly hereafter), respectively. In the first GI scheme, those two kinds of 1D phase-controlled sources are built by $N = 10$ equidistant slit sources and have the same physical unit $s_1 = 20$ and $s_2 = 2$. Figure 6(a) show the simulation result of the relationship between $(\mathrm{GI}/\mathrm{GI}_{\max})_{\min}$ and the window size W of the object. In Fig. 6(a), one can see that the visibility of ghost images with those two kinds of phase-controlled sources shows a downward trend along with a larger window size W. Compared with the Chaotic case, however, the Orderly case shows the advantage in visibility. The reason why the visibility of ghost images decreases with the increase of W is that the background superposition reduces the signal-to-noise ratio of GI from each points in the object. The larger the object, the more valid points ghost image contains. For the chaotic case, when the object is approximate to a single point, $(\mathrm{GI}/\mathrm{GI}_{\max})_{\min}$ is 0.5 which is consistent with the theoretic results the background-peak ratio 1/2 in the second-order bunching effect.

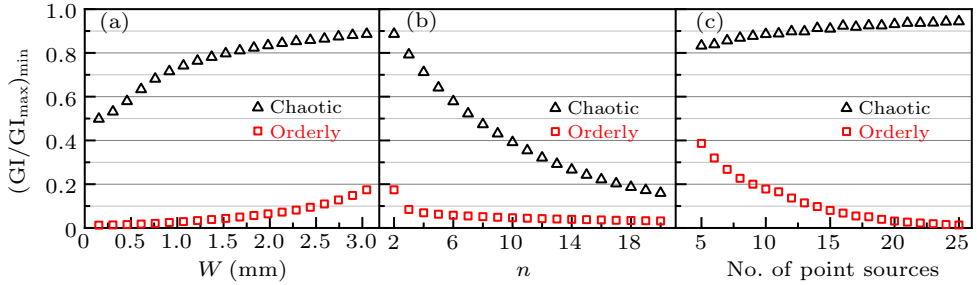


Fig. 6. Numerical simulation results of the minimum of normalized ghost image $(\mathrm{GI}/\mathrm{GI}_{\max})_{\min}$ with two kinds of 1D phase-controlled sources: the independent chaotic point sources (abbreviated as chaotic shown by the black hollow triangles) and the orderly phase-correlated sources (abbreviated as orderly shown by the red hollow squares), respectively. (a) The relationship between $(\mathrm{GI}/\mathrm{GI}_{\max})_{\min}$ and the window size W of the object. (b) Performance of the n-order GI. (c) The relationship between the second-order GI and the total point number in the 1D phase-controlled sources. Herein, the window size W of the object in panels (b) and (c) is 3.05 mm.

The visibility of GI results can be improved by the high-order imaging algorithm. Compared with the first GI scheme, the physical unit of sources in the second GI scheme is exactly same except the window size W of the object was fixed at 3.05 mm. Figure 6(b) shows the performance of the n-order $(\mathrm{GI}/\mathrm{GI}_{\max})_{\min}$ with those two kinds of phase-controlled sources. One can note that the visibility of n-order GI with those two kinds of phase-controlled sources can enhance as n increases. In practice, the number of exposure frames is very huge for suppressing the noise amplification in the conventional high-order GI algorithm.

The physical size of the source will influence the spatial resolution of the GI system. For discrete light sources, the number of point sources will determine the spatial bandwidth product of the imaging system.[20] Compared with the phase-controlled sources in the second GI scheme, the physical unit $s_1 = 20$ and $s_2 = 2$ is unchanged but the total number of points has been adjusted in the third GI scheme. By adjusting the number of point sources from 5 to 25, figure 6(c) shows the relationship between the point number and the visibility

of second-order GI with those two kinds of phase-controlled sources. Here, the window size W of the object was fixed at 3.05 mm. For the chaotic case, although the ratio 1/2 of the bunching background-to-peak has nothing to do with the number of point sources, the quantity of speckle particles illuminated on the object increases due to the improvement of spatial resolution of the GI system and leads to the imaging visibility decrease. However, for the orderly case, the decay of the bunching background-to-peak makes the visibility of the ghost image improve rapidly although the GI scheme's resolution is improved. In a word, the orderly phase-correlated sources in the above three GI schemes always show visibility superiority than the chaotic case.

5. Conclusion

In conclusion, firstly we theoretically compared the far-field second-order interference of independent chaotic point sources, orderly phase-correlated sources, and disorderly phase-correlated sources, respectively. We find that whether the arithmetic progression phase is arranged orderly or not, the super-bunching effect originate from the phase-correlated sources always appears. At the same time, we find that the second-order interference fringes originated from disorderly phase-correlated sources do not satisfy the space translation invariance, which is a necessary condition for the GI scheme established. Secondly, we created experimentally the orderly phase-correlated discrete sources which can realize the high-visibility second-order GI than the chaotic case. Finally, we discuss some factors that affect the visibility of GI and show that the orderly phase-correlated discrete sources are superior to the chaotic sources in terms of GI visibility.

Acknowledgement

Project supported by the National Natural Science Foundation of China (Grant No. 62105188).

References

[1] Moreau P A, Toninelli E, Gregory T and Padgett M J 2018 *Laser & Photon. Rev.* **12** 1700143
[2] Padgett M J and Boyd R W 2017 *Philos. Trans. R. Soc. A* **375** 20160233
[3] Wang C, Zhang D, Bai Y and Chen B 2010 *Phys. Rev. A* **82** 063814
[4] Meyers R, Deacon K S and Shih Y 2008 *Phys. Rev. A* **77** 041801
[5] Goodman J 1995 *Introduction to Fourier Optics* (Roberts and Company Publishers)
[6] Shapiro J H 2008 *Phys. Rev. A* **78** 061802
[7] Bromberg Y, Katz O and Silberberg Y 2009 *Phys. Rev. A* **79** 053840
[8] Katz O, Bromberg Y and Silberberg Y 2009 *Appl. Phys. Lett.* **95** 131110
[9] Pittman T B, Shih Y H, Strekalov D V and Sergienko A V 1995 *Phys. Rev. A* **52** R3429(R)
[10] Bennink R S, Bentley S J and Boyd R W 2002 *Phys. Rev. Lett.* **89** 113601
[11] Bennink R S, Bentley S J, Boyd R W and Howell J C 2004 *Phys. Rev. Lett.* **92** 033601
[12] Gatti A, Brambilla E, Bache M and Lugiato L A 2004 *Phys. Rev. A* **70** 013802
[13] Ferri F, Magatti D, Gatti A, Bache M, Brambilla E and Lugiato L A 2005 *Phys. Rev. Lett.* **94** 183602
[14] Valencia A, Scarcelli G, D'Angelo M and Shih Y 2005 *Phys. Rev. Lett.* **94** 063601
[15] Zhang D, Zhai Y H, Wu L A and Chen X H 2005 *Opt. Lett.* **30** 2354
[16] Brown R H and Twiss R Q 1956 *Nature* **177** 27
[17] Brown R H and Twiss R Q 1956 *Nature* **178** 1046
[18] Li L, Hong P and Zhang G 2019 *Phys. Rev. A* **99** 023848
[19] Basano L and Ottonello P 2007 *Am. J. Phys.* **75** 343
[20] Li L, Wang B, Li S, Yuan H and Xing F 2021 *Phys. Lett. A* **420** 127749
[21] Basano L and Ottonello P 2007 *Appl. Opt.* **46** 6291
[22] Ferri F, Magatti D, Lugiato L A and Gatti A 2010 *Phys. Rev. Lett.* **104** 253603
[23] Chen H, Peng T and Shih Y 2013 *Phys. Rev. A* **88** 023808
[24] Chen X H, Yan L, Wu W, Meng S Y, Wu L A, Sun Z B, Wang C and Zhai G J 2017 *Chin. Phys. B* **26** 060702
[25] Li Y and Duan D 2023 *Chin. Phys. B* **32** 104203
[26] Liu X F, Li M F, Yao X R, Yu W K, Zhai G J and Wu L A 2013 *AIP Advances* **3** 052121
[27] Luo C and Cheng J 2013 *Opt. Lett.* **38** 5381
[28] Liu R, Fang A, Zhou Y, Zhang P, Gao S, Li H, Gao H and Li F 2016 *Phys. Rev. A* **93** 013822
[29] Si Y, Kong L J, Li Y N, Tu C H and Wang H T 2016 *Chin. Phys. Lett.* **33** 034203
[30] Liu Z Q, Bai Y F, Zou X P F, Zhou L Y, Fu Q and Fu X Q 2023 *Chin. Phys. B* **32** 034210
[31] Bai Y and Han S 2007 *Phys. Rev. A* **76** 043828
[32] Agafonov I N, Chekhova M V, Iskhakov T S and Penin A N 2008 *Phys. Rev. A* **77** 053801
[33] Cao D Z, Xiong J, Zhang S H, Lin L F, Gao L and Wang K 2008 *Appl. Phys. Lett.* **92** 201102
[34] Chan K W C, O'Sullivan M N and Boyd R W 2009 *Opt. Lett.* **34** 3343
[35] Liu Q, Chen X H, Luo K H, Wu W and Wu L A 2009 *Phys. Rev. A* **79** 053844
[36] Chen X H, Agafonov I N, Luo K H, Liu Q, Xian R, Chekhova M V and Wu L A 2010 *Opt. Lett.* **35** 1166
[37] Zhou Y, Simon J, Liu J and Shih Y 2010 *Phys. Rev. A* **81** 043831
[38] Chen X H, Chen W, Meng S Y, Wu W, Wu L A and Zhai G J 2013 *J. Opt. Soc. Am. A* **30** 1422
[39] Ou L H and Kuang L M 2007 *J. Phys. B: At. Mol. Opt. Phys.* **40** 1833
[40] Agafonov I N, Chekhova M V, Iskhakov T S and Wu L A 2008 *J. Mod. Opt.* **56** 422
[41] Liu J and Shih Y 2009 *Phys. Rev. A* **79** 023819
[42] Li H G, Zhang Y T, Cao D Z, Xiong J and Wang K G 2008 *Chin. Phys. B* **17** 4510
[43] Hong P and Zhang G 2017 *Opt. Express* **25** 22789
[44] Wang C, Lan R J, Ren C and Cao D Z 2020 *Phys. Rev. A* **101** 033819
[45] Hong P, Liu J and Zhang G 2012 *Phys. Rev. A* **86** 013807
[46] Bromberg Y and Cao H 2014 *Phys. Rev. Lett.* **112** 213904
[47] Zhou Y, Li F, Bai B, Chen H, Liu J, Xu Z and Zheng H 2017 *Phys. Rev. A* **95** 053809
[48] Bai B, Liu J, Zhou Y, Zheng H, Chen H, Zhang S, He Y, Li F and Xu Z 2017 *J. Opt. Soc. Am. B* **34** 2081
[49] Bender N, Yilmaz H, Bromberg Y and Cao H 2018 *Optica* **5** 595
[50] Zhang L, Lu Y, Zhou D, Zhang H, Li L and Zhang G 2019 *Phys. Rev. A* **99** 063827
[51] Mandel L 1983 *Phys. Rev. A* **28** 929
[52] Scully M O and Zubairy M S 1997 *Quantum Optics* (Cambridge University Press)
[53] Shih Y 2011 *An Introduction to Quantum Optics: Photon and Biphoton Physics* (CRC Press)
[54] Fano U 1961 *Am. J. Phys.* **29** 539
[55] Liu J and Zhang G 2010 *Phys. Rev. A* **82** 013822
[56] Hong P and Zhang G 2013 *Phys. Rev. A* **88** 043838
[57] Hong P, Xu L, Zhai Z and Zhang G 2013 *Opt. Express* **21** 14056
[58] Greenberger D M, Horne M A and Zeilinger A 1993 *Phys. Today* **46** 22
[59] Liu J and Zhang G 2011 *Opt. Commun* **284** 2658